JOURNAL OF CATALYSIS **164,** 440–448 (1996)
ARTICLE NO. 0400

# Zirconium Oxides Dispersed on Silica Derived from $Cp_2ZrCl_2$, $[(i\text{-}PrCp)_2ZrH(\mu\text{-}H)]_2$, and $Zr(OEt)_4$ Characterized by X-Ray Absorption Fine Structure and Catalytic Ketonization of Acetic Acid

K. Okumura and Y. Iwasawa[1]

*Department of Chemistry, Graduate School of Science, The University of Tokyo, Hongo, Bunkyo-ku, Tokyo 113, Japan*

Received May 1, 1996; revised August 26, 1996; accepted September 11, 1996

**Newly dispersed Zr oxides on $SiO_2$ were prepared from $Cp_2ZrCl_2$, $[(i\text{-}PrCp)_2ZrH(\mu\text{-}H)]_2$, and $Zr(OEt)_4$ precursors and were characterized by X-ray absorption fine structure (XAFS) and catalytic ketonization of acetic acid. $ZrCp_2Cl_2$ and $[(i\text{-}PrCp)_2ZrH(\mu\text{-}H)]_2$ precursors yielded monomeric Zr oxides with unsaturated coordination in low loadings, whereas $Zr(OEt)_4$ yielded Zr-oxide assemblies in octahedral symmetry independent of Zr loading up to 15 wt% Zr. The former catalysts were more active than the latter catalyst for ketonization of acetic acid. The catalytic ketonization was suggested to proceed via bidentate acetates adsorbed on neighboring Zr sites.** 

## INTRODUCTION

Ketonization of carboxylic acids has attracted much attention for applications in synthesizing asymmetric ketones (1) as well as for fundamental interests such as the intermediates and mechanism of the carbon number-increasing reaction (2). Ketonization of carboxylic acids can also be used as a probe reaction to investigate correlation between surface structure and catalytic properties of metal oxides. Many kinds of oxides have been reported to be active for this reaction and have been classified into two categories: one is the metal oxides such as groups 1 and 2 in the periodic table, which are converted to the carboxylate salts even inside the bulk under reaction conditions, and the other is the metal oxides whose surfaces are only transformed to the carboxylate ions (3–5). Different mechanisms for ketonization of carboxylic acids have been proposed thus far (6): e.g., (a) an acid anhydride intermediate (7), (b) a $\beta$-keto acid intermediate (two unidentate carboxylates and $\alpha$-hydrogen abstraction) (8), (c) a concerted mechanism involving two unidentate carboxylates (9), (d) a molecular carboxylic acid intermediate (10), (e) carboxylate ions (3, 11, 12) (f) a carboxylate ion–carboxylic acid reaction (13), (g) a ketene intermediate which reacts with carboxylate ions (13, 14), and (h) an acyl carbonium ion (protonated ketene) intermediate which reacts with carboxylic ions (11, 15, 16). Among these proposed mechanisms, the bimolecular reaction between either two adsorbed acetate ions or one adsorbed acetate ion and an adsorbed acyl carbonium ion may be the mechanism responsible for ketonization of acetic acid (6).

It has been demonstrated that $ZrO_2$ shows unique catalysis for the hydrogenation reactions of carbon monoxide and ethene, and the dehydrogenation of butanamine (17–23). Recently, much effort has been directed to sulfated $ZrO_2$ which shows a super acid character (24–32).

Yakerson *et al.* (33) investigated acetic acid decomposition on tetravalent oxides and reported the order of activity $CeO_2 > ZrO_2 > TiO_2 > SnO_2$. In this series, $CeO_2$ shows the highest activity, but the reduction from $Ce^{4+}$ to $Ce^{3+}$ occurs under the reaction conditions, leading to the destruction of the catalyst. Hence $ZrO_2$ is regarded to be a superior catalyst.

Dispersed oxides and monolayer oxides often show different catalytic properties from each other and also from the bulk property, due to the different structures of their oxidic metal sites (34–36). Dispersed and monolayer oxides supported on high surface-area oxides like $SiO_2$ by using metal organics as precursors have advantages for the development of new catalytic systems and interfaces and also in fundamental research of catalytic reaction mechanisms (37–39). In most cases of supported $ZrO_2$ catalysts prepared by a conventional impregnation method using inorganic zirconium salts, segregation or large particles of $ZrO_2$ are observed on support surfaces and control of the dispersion is difficult (40, 41).

In this study, we report the preparation of Zr oxides dispersed on silica prepared by $Cp_2ZrCl_2$, $[(i\text{-}PrCp)_2ZrH \cdot (\mu\text{-}H)]_2$, and $Zr(OEt)_4$, their characterizations, and the catalytic properties for ketonization of acetic acid to form acetone.

[1] To whom correspondence should be addressed.



0021-9517/96 $18.00

## EXPERIMENTAL

### *Catalyst Preparation from $Cp_2ZrCl_2$*

Silica (Silica gel No. 952 (Fuji Davison); 250 $m^2\ g^{-1}$) was calcined at 673 K for 1 h, followed by evacuation at the same temperature for 0.5 h before its use as the support. The $SiO_2$ was impregnated with a toluene solution of $Cp_2ZrCl_2$ for 1.5 h under an Ar (99.9999%) atmosphere at room temperature, followed by evacuation to remove the solvent. The samples thus obtained were calcined at 773 K for 1 h in air. The Zr loading was varied in the range 1.5–8.4 wt% as $Zr/SiO_2$. The catalysts prepared from $Cp_2ZrCl_2$ are denoted as catalyst A.

### *Catalyst Preparation from $Zr(OEt)_4$*

Zirconium ethoxide $Zr(OEt)_4$ vapor was deposited on silica (silica gel No. 952) in a manner similar to that reported previously (35). $SiO_2$ was evacuated at 573 K and mixed with a given amount of $Zr(OEt)_4$ powder in an Ar (99.9999%) atmosphere. After evacuation, the samples were heated to 473 K for 1.5 h while stirring vigorously. The obtained samples were then calcined at 773 K for 1 h before being used as a catalyst. The catalysts with Zr loadings of less than 11.7 wt% were prepared by this procedure. Repeating the above procedure to prepare the higher loading samples was necessary because of the large molecular size of $Zr(OEt)_4$, which covers the $SiO_2$ surface upon adsorption, and the remaining moiety of the Zr species after reaction with the surface OH groups prevents the $Zr(OEt)_4$ from further interacting with the unreacted OH groups of the $SiO_2$ surface. The loading was determined from the weight gain of the sample with the assumption that the calcined Zr had the composition of $ZrO_2$, and also by x-ray fluorescence analysis, which coincided with the loading expected from the weight of the $Zr(OEt)_4$. These catalysts are denoted as catalyst B.

### *Catalyst Preparation from $[(i\text{-}PrCp)_2ZrH(\mu\text{-}H)]_2$*

A zirconium dimer complex $[(i\text{-}PrCp)_2ZrH(\mu\text{-}H)]_2$ was synthesized according to the literature (42). Special care was paid to the handling of this complex because of its high sensitivity to air. The procedure of catalyst preparation was similar to that described for catalyst A except for the use of hexane as the solvent. These catalysts are denoted as catalyst C.

### *XAFS Spectra Measurement*

Zr *K*-edge x-ray absorption fine structure (XAFS) spectra were measured in a transmission mode at room temperature with the beam line 10B or 7C of the Photon Factory in the National Laboratory for High-Energy Physics (KEK-PF) (Proposal No. 92-009). The storage ring energy was operated at 2.5 GeV with a current of 250–350 mA. The catalysts were transferred to glass cells equipped with two capton windows. Two ion chambers, one filled with Ar 50%/$N_2$ 50% and the other with Ar 100%, were used as detectors for $I_0$ and I, respectively.

For extended x-ray absorption fine structure (EXAFS) analysis, the oscillation was extracted from the EXAFS data by a cubic spline method and normalized with the edge height. The Fourier transformation of the $k^3$-weighted EXAFS oscillation from *k* space to *R* space was performed over the range 30–130 $nm^{-1}$. The inversely Fourier filtered data were analyzed by a curve fitting method. The phase shift and amplitude parameters were extracted from Zr foil and $Zr(acac)_4$ for Zr–Zr and Zr–O, respectively. For Zr–Si, we used the theoretical parameter calculated from FEFF 6.0 (43). Error bars of the analysis were estimated by *R* factor ($R_f$) defined as

$$R_f = \int \left|k^3\chi(k)^{obs} - k^3\chi(k)^{calc}\right|^2 dk \Big/ \int \left|k^3\chi(k)^{obs}\right|^2 dk.$$

The error bars of the bond distance and coordination number determined by the present curve fitting analysis are estimated to be about 0.002 nm and 20%, respectively, as shown in Table 1.

### *FTIR Measurement*

Infrared spectra were measured on a JASCO FT-IR 230 spectrometer with a resolution of 2 $cm^{-1}$. The sample (60 mg wafer, diameter 2 cm) was placed in an IR cell with two NaCl windows which was combined with a closed circulating system for measurements of the spectra *in situ* under the catalytic reaction conditions.

### *Catalytic Reaction*

Catalytic ketonization reactions, $2CH_3COOH \rightarrow CH_3COCH_3 + CO_2 + H_2O$, were carried out in a closed circulating system (dead volume 200 $cm^3$). The catalyst was placed in a U-shaped tube in the system and calcined at 773 K for 1 h before each reaction. Acetic acid (0.1–1.0 kPa) mixed with helium (13.3 kPa) was introduced into the system. The products at the reaction at temperatures of 423–623 K were analyzed by an on-line gas chromatograph (columns were Porapak T and Porapak PS).

### *Temperature Programmed Desorption (TPD) Measurement*

TPD spectra were carried out in a closed circulating system. The catalyst adsorbed with acetic acid was placed in a U-shaped tube of the circulating system and heated at a rate of 4 K $min^{-1}$ to 723 K. The desorbed products were collected by a liquid $N_2$ trap and analyzed with a gas chromatograph.

**TABLE 1**

**Curve Fitting Results of the EXAFS Data for Catalysts A, B, and C**

| Catalyst | Scatterer atom | CN[a] | R/nm[b] | $\Delta E_0$/eV[c] | $\sigma$/nm[d] | $R_f$/%[e] |
|---|---|---|---|---|---|---|
| A | | | | | | |
| 1.5 wt% | O | 1.5 ± 0.2 | 0.199 ± 0.001 | −8.0 ± 4.0 | 0.0038 ± 0.0014 | |
| | O | 3.0 ± 0.7 | 0.260 ± 0.002 | −14.2 ± 4.0 | 0.0095 ± 0.0018 | |
| | Si | 1.6 ± 0.3 | 0.338 ± 0.001 | 3.0 ± 2.0 | 0.0090 ± 0.0009 | 3.4 |
| 2.3 wt% | O | 1.5 ± 0.2 | 0.201 ± 0.001 | −6.5 ± 4.0 | 0.0038 ± 0.0014 | |
| | O | 3.0 ± 0.7 | 0.260 ± 0.002 | −14.8 ± 4.0 | 0.0095 ± 0.0018 | |
| | Si | 1.7 ± 0.3 | 0.338 ± 0.001 | 3.0 ± 2.0 | 0.0090 ± 0.0009 | 4.2 |
| 4.5 wt% | O | 5.1 ± 1.6 | 0.211 ± 0.002 | −1.9 ± 4.0 | 0.0101 ± 0.0013 | |
| | Si | 1.4 ± 0.4 | 0.338 ± 0.002 | 3.5 ± 2.0 | 0.0085 ± 0.0012 | |
| | Zr | 1.2 ± 0.3 | 0.359 ± 0.001 | 2.1 ± 5.0 | 0.0087 ± 0.0013 | 7.9 |
| B | | | | | | |
| 1.4 wt% | O | 8.8 ± 2.3 | 0.213 ± 0.002 | 2.9 ± 5.0 | 0.0126 ± 0.0013 | |
| | Si | 2.3 ± 0.4 | 0.339 ± 0.001 | 1.4 ± 3.0 | 0.0107 ± 0.0010 | 4.0 |
| 1.4 wt% | O | 6.3 ± 1.4 | 0.213 ± 0.002 | 1.1 ± 4.0 | 0.0105 ± 0.0014 | |
| with acetic acid | Si | 1.0 ± 0.2 | 0.333 ± 0.002 | −3.2 ± 3.0 | 0.0073 ± 0.0015 | |
| | Zr | 1.0 ± 0.3 | 0.363 ± 0.001 | 5.0 ± 5.0 | 0.0093 ± 0.0012 | 7.4 |
| 11.7 wt% | O | 8.8 ± 2.3 | 0.215 ± 0.002 | 3.6 ± 5.0 | 0.0131 ± 0.0013 | |
| | Si | 2.4 ± 0.4 | 0.341 ± 0.001 | 2.5 ± 3.0 | 0.0103 ± 0.0010 | 1.5 |
| 15.0 wt% | O | 8.0 ± 2.3 | 0.215 ± 0.002 | 3.3 ± 5.0 | 0.0122 ± 0.0013 | |
| | Si | 2.4 ± 0.4 | 0.345 ± 0.001 | 4.6 ± 3.0 | 0.0107 ± 0.0010 | 2.6 |
| C | | | | | | |
| 1.7 wt% | O | 1.7 ± 0.2 | 0.200 ± 0.001 | −11.3 ± 4.0 | 0.0035 ± 0.0014 | |
| | O | 3.0 ± 0.7 | 0.262 ± 0.002 | −11.2 ± 4.0 | 0.0105 ± 0.0018 | |
| | Si | 2.1 ± 0.3 | 0.337 ± 0.001 | 1.9 ± 2.0 | 0.0108 ± 0.0009 | 7.8 |

[a] Coordination number.
[b] Bond distance.
[c] Energy difference of the origin of photoelectron from the reference.
[d] Debye-Waller factor.
[e] Residual factor.

## RESULTS AND DISCUSSION

### *Structure of Catalysts A*

In the x-ray absorption near-edge structure (XANES) spectrum of catalyst A prepared by $Cp_2ZrCl_2$ precursor a characteristic pre-edge peak was observed as shown in Fig. 1. The pre-edge XANES peak originates from the transition from 1*s* to 4*d* that is enhanced by *d–p* orbital mixing. Thus the pre-edge peak can be observed with tetrahedral geometry around the Zr center rather than octahedral symmetry. Indeed, tetragonal $ZrO_2$, whose structure is regarded as having eight coordination composed of two sets of nonequivalent Zr–O tetrahedra, shows merely a small shoulder at the Zr *K*-edge XANES in Fig. 1 (44). Thus catalyst A is likely to possess Zr sites in near-tetrahedral symmetry or at least in a geometry less coordinated than octahedral symmetry. This pre-edge peak disappeared after the introduction of acetic acid vapor to the catalyst at room temperature as shown in Fig. 1b, which was similar to the XANES spectrum for $BaZrO_3$ with octahedral symmetry around Zr. It was not possible to quantitatively compare the pre-edge peak of the sample with standard compounds because of the lack of tetrahedral Zr-oxide compounds. Nevertheless these results demonstrate that acetic acid adsorbed on the coordinatively unsaturated Zr sites increases the coordination number around the Zr atoms.

Figure 2 shows the Zr *K*-edge EXAFS Fourier transforms for catalysts A with different Zr loadings and also for monoclinic bulk $ZrO_2$. The peak observed at 0.15–0.17 nm in the Fourier transforms (phase shift uncorrected) for all supported samples are straightforwardly assigned to the Zr–O bond as compared with that for the bulk $ZrO_2$. However, Zr–Zr bonding observed with $ZrO_2$ is not seen or is unclear for catalyst A. As for the 1.5 and 2.3 wt% samples, a small peak at 0.29 nm (phase shift uncorrected) was observed. This peak might be due to the Zr–Zr bond, but this possibility was excluded because the peak was too short to be assigned as the Zr–Zr bond in Zr oxides and no curve fitting was successful if the peak was assumed to be Zr–Zr bond. The origin of the peak below 0.1 nm observed in the Fourier transform is not due to real bonding, but occurred in the process of extracting the EXAFS oscillation without a phase shift correction by the cubic spline method. We performed the EXAFS curve fitting analysis over the whole

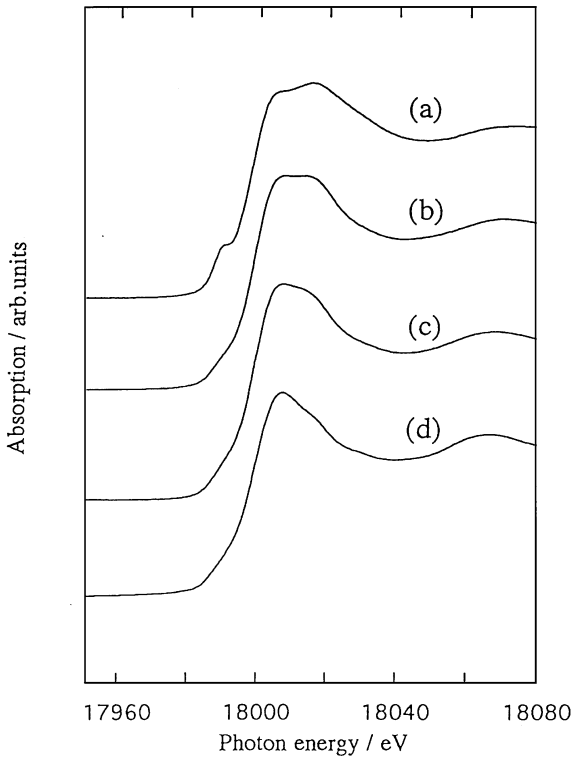


**FIG. 1.** XANES spectra of (a) catalyst A 1.5 wt%, (b) catalyst A (1.5 wt%) after exposure to 1.3 kPa acetic acid, (c) catalyst B 1.7 wt%, and (d) $ZrO_2$.

range 0.11–0.36 nm including the peak around 0.2 nm. In this case the number of the independent parameter $N_I = 2\Delta R\Delta k/\pi + n (n = 1$ or 2) is calculated to be 15 or 16, which would mean allowing fitting waves up to three or four. The three-waves fitting Zr–O + Zr–O + Zr–Si) reproduced the observed EXAFS data as shown in Figs. 3a and 3b. No analysis using two waves (Zr–O + Zr–Si) fitted the data at all. The best fit results for the catalysts A (1.5 and 2.3 wt%) are shown in Table 1. The absence of Zr–Zr and the presence of Zr–Si imply a direct bond formation of Zr with the silica surface in a monomeric Zr form. The catalysts A with 1.5 and 2.3 wt% Zr showed almost the same EXAFS oscillation, while the catalyst A with 4.5 wt% Zr showed a different oscillation and a new peak appeared around 0.33 nm (phase shift uncorrected) as seen in Fig. 2c. This peak was assigned to the Zr–Zr bond by the curve fitting method. It is known that there exist three phases of $ZrO_2$, that is, the monoclinic, tetragonal, and cubic phases. The monoclinic phase is stable below 1443 K, but the metastable tetragonal phase also can exist at room temperature when its size is small (45). The Zr–Zr distance is 0.345 nm for monoclinic (46) and 0.366 nm for tetragonal $ZrO_2$ (47). The Zr–Zr distance for the catalyst A with 4.5 wt% Zr was determined to be 0.359 nm, which is closer to the 0.364 nm of the tetragonal structure rather than the 0.345 nm of the monoclinic structure, although the Zr–Zr bond distance for the catalyst A cannot be directly compared to the bulk $ZrO_2$ crystals because the Zr oxide species in the catalyst A does not grow to three-dimensional particles. The coordination number of the Zr–Zr bond was as small as 1.2, which suggests the formation of small clusters of tetragonal-like Zr oxide, probably dimers on the $SiO_2$ surface. The coordination number of the Zr–Si bond did not change much upon increasing Zr-loading from 1.5 to 4.5 wt%, as shown in Table 1. The bond distance of Zr–O for the 1.5 and 2.3 wt% catalysts A (0.199–0.201 nm) increased to 0.211 nm for the 4.5 wt% catalyst A, and the Zr–O peak became broader. This feature also coincides with the onset of the formation of the Zr–Zr bond. The difference in the bond distance of Zr–O between the 1.5–2.3 wt% catalysts and the 4.5 wt% catalyst may be attributed to the differences of the local Zr structures. The shorter Zr–O bonds at 0.199–0.201 nm for the catalysts A with the low Zr loadings have not been reported thus far elsewhere, suggesting the unique structure of their Zr sites. The $ZrO_2$ phase deposited on $TiO_2$ by using Zr alkoxide has been reported to be monoclinic for high-loading Zr samples (45). This result is different from our observation that the structure is similar to the local structure of tetragonal $ZrO_2$ grown on $SiO_2$ at higher Zr loadings. It should be noted that the structure and nature of the support has a profound effect on the structure of the Zr oxide overlayers. We tentatively propose the structures of Zr sites for the catalyst A (1.5–2.3 and 4.5 wt%) based on EXAFS and XANES in Figs. 4a and 4b, respectively.

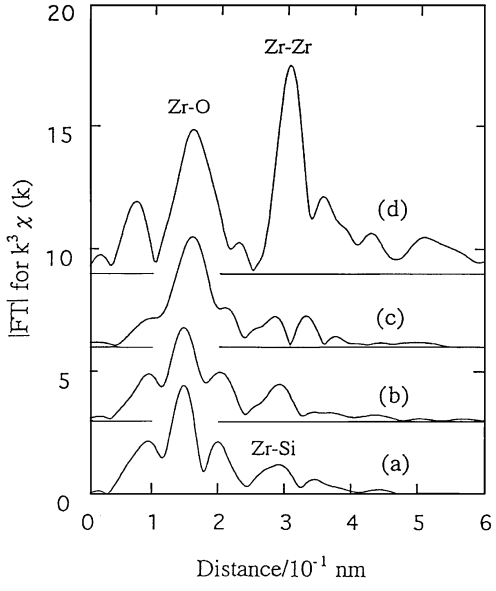


**FIG. 2.** EXAFS Fourier transforms (phase shift uncorrected) for catalysts A and $ZrO_2$: catalyst A (a) 1.5 wt%, (b) 2.3 wt%, and (c) 4.5 wt%, and (d) $ZrO_2$.

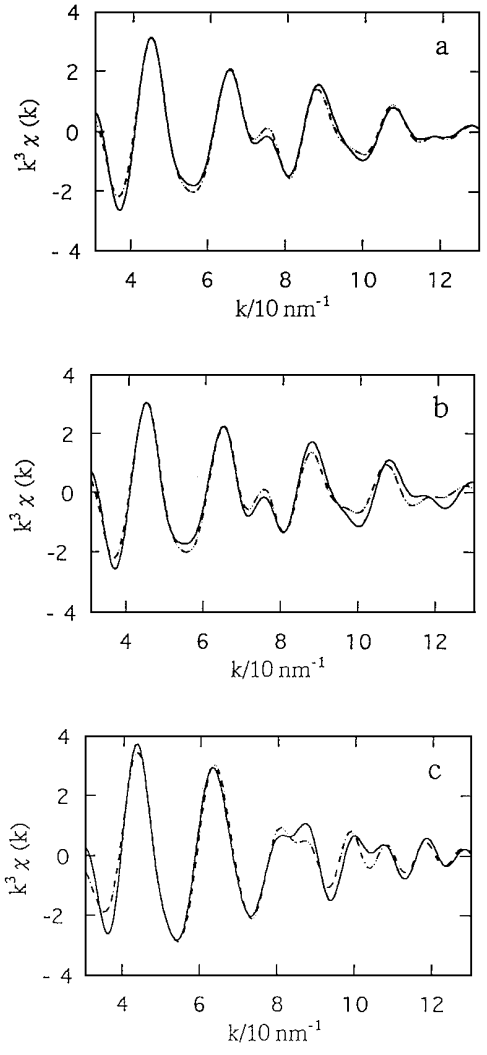


**FIG. 3.** Curve fitting results for the EXAFS data of catalysts A: (a) 1.5 wt%, (b) 2.3 wt%, and (c) 4.5 wt%.

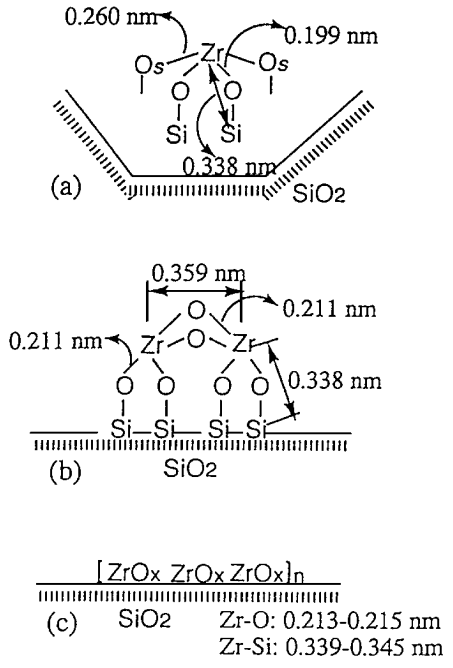


**FIG. 4.** Proposed structures of Zr sites for (a) catalyst A (1.5–2.3 wt%), (b) catalyst A (4.5 wt%), and (c) catalyst B (0.3–15.0 wt%).

*Structure of Catalysts B*

The XANES spectrum of catalyst B is also shown in Fig. 1. The characteristic pre-edge peak observed with catalyst A did not appear for catalyst B even at low loading of Zr. The XANES spectra did not change by increasing Zr loading up to 15.0 wt%. Figure 5 shows the Fourier transform of EXAFS spectra for catalysts B with different Zr loadings. The best fit results over the whole 0.04–0.32 nm range in the Fourier transform spectra for the catalysts B are shown in Fig. 6 and listed in Table 1. In the Fourier transform the first peak is straightforwardly assigned to the Zr–O bond. The second peak around 0.3 nm (phase shift uncorrected) may be due to Zr–Zr and/or Zr–Si bonds. The curve fitting never reproduced the observed EXAFS data if the peak was assumed to be due to Zr–Zr bonding. The EXAFS data were well fitted only by Zr–Si bonding. The bond distances for Zr–O and Zr–Si were determined to be 0.213–0.215 and 0.339–0.345 nm, respectively, for the samples with 1.4–15.0 wt% Zr. These distances are a little longer than those for catalysts A. A more striking difference between catalyst A and catalyst B is seen in the coordination number of the Zr–O bond. The Zr–O coordination numbers for catalyst B are higher than those for catalyst A, indicating the high coordination geometry around a Zr atom in catalyst B, which coincides with the suggestion of an octahedral

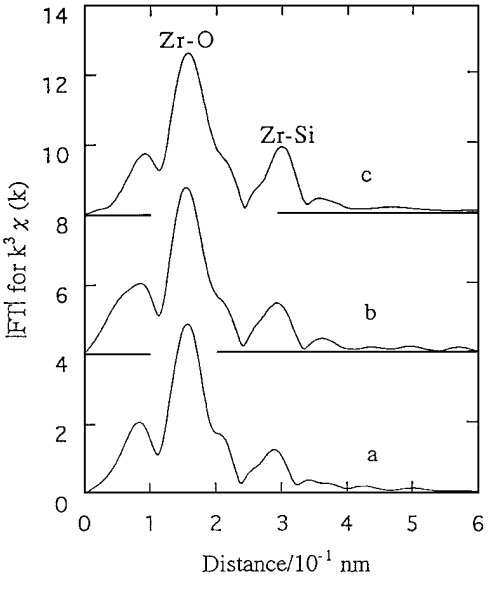


**FIG. 5.** EXAFS Fourier transforms for catalysts B: (a) 1.4 wt%, (b) 11.2 wt%, and (c) 15.0 wt%.

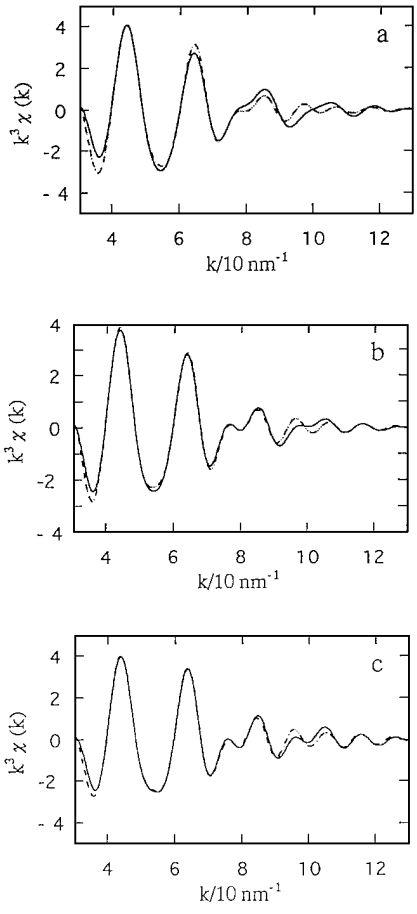


**FIG. 6.** Curve fitting results for the EXAFS data of catalysts B; (a) 1.4 wt%, (b) 11.2 wt%, and (c) 15.0 wt%.

symmetry from the XANES spectrum of Fig. 1. It should be noted that no Zr–Zr bonding was observed with catalyst B. These results mean bulk $ZrO_2$ does not grow on $SiO_2$, and the monomeric Zr oxide species are chemically bonded to the silica surface. This is contrary to the previous reports for $TiO_2/SiO_2$ (49) and $Nb_2O_5/SiO_2$ (50) which show one-atomic-layer growth with metal–metal bonds. The similar Zr–Si coordination number for all examined catalysts B suggests one-atomic-layer dispersion on silica independent of Zr loading (Fig. 4). Now if we assume that one $ZrO_2$ unit occupies a surface area of 0.13 nm$^2$, then the loading of one-atomic-monolayer $ZrO_2/SiO_2$ should reach 21 wt%. So the value 15.0 wt% corresponds to 71% of this full monolayer.

We tried to further react $Zr(OEt)_4$ with the 15.0 wt% Zr monolayer sample to make a full $ZrO_2$ monolayer on $SiO_2$, but epitaxial growth of the $ZrO_2$ monolayer did not succeed and only tetragonal $ZrO_2$ particles were formed as proved by XRD (51).

*Catalytic Ketonization of Acetic Acid*

The initial rates of carbon dioxide formation on catalysts A and catalysts B at 573 K were plotted against Zr loading in Fig. 7. The temperature-programmed desorption for surface acetates (adsorbed acetic acid) seen in Fig. 9 suggests that the acetone produced along with $CO_2$ in the ketonization was partially converted to ketene by a byreaction competitive with its desorption, though the $CO_2$/acetone ratio depended on the coverage of acetates. Therefore the rate of $CO_2$ formation was defined as the initial rate of the ketonization in this study. As for catalyst A, the activity (initial rate per gram Zr) increased linearly with an increase in the Zr loading up to ca. 4 wt%. The activity of catalyst A showed a maximum at an 8 wt% Zr loading, then decreased at higher loadings. We checked the activity of the $SiO_2$ support itself, but it was inactive for this reaction. The linear dependence of the initial rate ($v_0$) per gram Zr ([Zr]) on the Zr loading, $(v_0/[Zr]) \propto [Zr]$, in the low loading region in Fig. 7 implies that the reaction rate with catalyst A is proportional to the square of the amount of Zr supported on $SiO_2$. As described above, no Zr–Zr bonding was observed for the samples with 1.5 and 2.3 wt% Zr loadings. This is also the case for the catalyst C prepared from the Zr-dimer precursor as described hereinafter. It seems that the Zr atoms are more or less randomly distributed on the $SiO_2$ surface because the species formed during calcination of the incipient supported complexes may migrate on the surface. Thus the probability of the formation of Zr pair sites on the surface will be proportional to the number of Zr sites squared, where two Zr sites contribute to the ketonization of acetic acid. The activity of the catalyst A with 8 wt% Zr deviated from the linear dependency probably due to a change of the local structure around the Zr atom. The EXAFS analysis for this catalyst was not successfully performed, probably because there were more than two different Zr structures on the $SiO_2$. The EXAFS spectrum for the catalyst A with

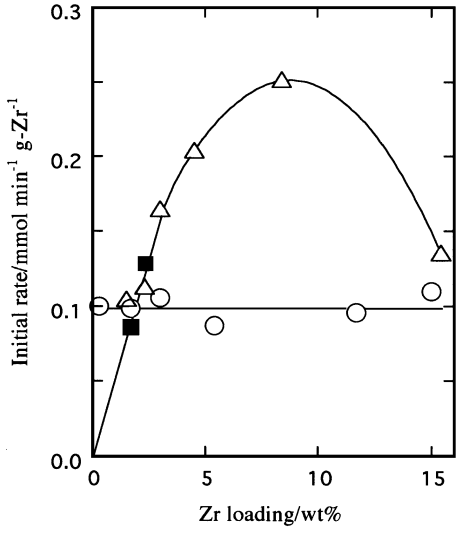


**FIG. 7.** Variation of the initial rate for acetic acid decomposition with Zr loading: acetic acid pressure, 0.9 kPa; reaction temperature, 573 K. (△) catalyst A, (○) catalyst B, (■) catalyst C.

15.5 wt% Zr was similar to that for the catalyst B with 15.0 wt% Zr. In fact, the catalyst A with 15.5 wt% Zr showed activity similar to that of the catalyst B, as shown in Fig. 7.

The initial rate per gram Zr for catalyst B was independent of the Zr loading over a wide range, as shown in Fig. 7, suggesting almost the same activity for each Zr site. This result coincides with the fact that the catalysts B show similar structures around Zr sites over a wide range of Zr loading in Table 1.

Acetic acid adsorbs as unidentate acetate on $SiO_2$, with a characteristic IR peak at 1756 $cm^{-1}$. On the other hand, the majority of adsorbed species on the catalyst B with 15.0 wt% Zr was bidentate acetate which had an asymmetric OCO stretching peak at 1556 $cm^{-1}$ and a symmetric OCO stretching peak at 1452 $cm^{-1}$. The unidentate acetate peak on $SiO_2$ was minor, as expected from the Zr coverage of 71% at the surface. A similar observation of the bidentate was reported for formic acid adsorbed on $ZrO_2$ (52).

The possibility of a reaction between the acetate on Zr and molecular acetic acid was examined under the reaction conditions of the saturated coverage of the acetate while the pressure of the acetic acid in the gas phase was being changed. The catalyst surface was saturated with the acetates in the pressure ranges 0.1–1.0 kPa as proved by the IR peak for acetate species on Zr that was independent of the pressure of acetic acid in the gas phase. The rate of ketonization did not depend on the acetic acid pressure in the range 0.1–1.0 kPa, which may exclude the participation of molecular acetic acid in the key step of the ketonization.

Figure 8 shows the change of the normalized intensities of bidentate and unidentate acetates on catalysts A and B at 623 K under 13.3 kPa He in a closed circulating system as a function of reaction time. After steady-state ketonization at 673 K for 10 min, the gas phase products were trapped with a liquid $N_2$ trap, followed with behaviors of the unidentate and bidentate acetates, and measuring the peak intensity at 1756 and 1556 $cm^{-1}$, respectively, in the absence of the gas-phase acetic acid. The peak intensities were normalized to those at the 10-min steady-state reaction in Fig. 8. A relatively fast decrease in the time profile was observed at the initial stage of reaction, followed by a slower decrease in the intensities. The reaction rate calculated from the initial slope of the peak decrease, assuming that the reaction taking place is from two adsorbed acetates, was consistent with the initial rate of the catalytic reaction. The agreement indicates that the ketonization of acetic acid takes place at the surface between two acetate species. A similar result was also obtained with the 18.7 wt% Zr catalyst B, for which only bidentate acetates were observed. Thus it is likely that the catalytic ketonization of acetic acid proceeds directly or indirectly between two bidentate acetates. Both bidentate and unidentate acetates existed on the 2.3 wt% Zr catalyst A and decreased in a similar way as a function of reaction time in Fig. 8. The unidentate acetates on $SiO_2$ carrier seem to move on Zr sites to form the bidentate acetates under the reaction conditions. The other species such as acyl cation and anhydride were not observed at any temperature.

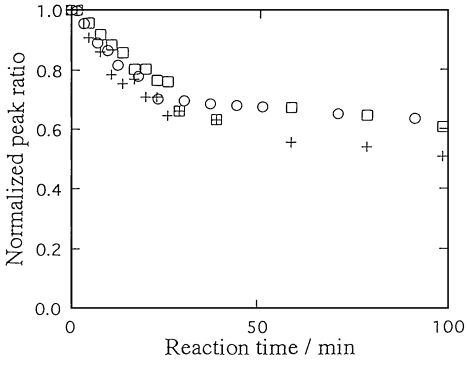


**FIG. 8.** Normalized peak intensity change of uni- and bidentate acetates in IR spectra during the surface reaction, while trapping acetic acid: (□) bidentate acetate on catalyst A, 2.3 wt%; (+) unidentate acetate on catalyst A, 2.3 wt%; (◯) bidentate acetate on catalyst B, 15.0 wt%.

It is presumed that the ketonization of acetic acid on the catalysts A and B is facilitated by two neighboring Zr sites which posses bidentate acetate ions. As shown in Fig. 7, the activity in the low Zr-loading region increased in proportion to the square of the Zr quantity on $SiO_2$. We followed the observation of direct Zr–Zr bonding (coordination number 1.2) between the adjacent Zr sites int he catalyst A with 4.5 wt% Zr with the EXAFS analysis shown in Table 1. As the linear relationship between the catalytic activity and the square of the Zr quantity follows up to about 4.5 wt% loading, as shown in Fig. 7, it is likely that the ketonization on catalysts A with low Zr loadings proceeds by two bidentate acetates on the adjacent Zr sites.

The Zr oxides in the catalysts B are supported in a two-dimensional dispersed form up to 15.0 wt% loading as discussed above. Although direct Zr–Zr bonding was not detected under vacuum, a Zr–Zr bond was observed when the catalyst B with 1.4 wt% Zr was exposed to acetic acid vapor at room temperature, as shown in Table 1. This indicates that the Zr sites in the catalyst B are also located in the neighborhood of each other. The higher activity of catalyst B with 0.3 wt% Zr as compared to the corresponding low-loading catalyst A may result from the formation of a Zr-oxide assembly rather than from isolated species even at the low loading. The size and structure of the Zr-oxide ensemble in catalysts B seem to be similar for the whole range of Zr loading from 0.3 to 15.0 wt%. The aggregation of Zr sites in catalyst B prepared from $Zr(OEt)_4$ is advantageous for the bimolecular reaction at the low Zr loading, while this advantage is lost at the high Zr loading because the population of the adjacent Zr sites in the catalyst A prepared from a monomeric complex $Cp_2ZrCl_2$ increases with an increase of Zr loading, where the coordinatively unsaturated

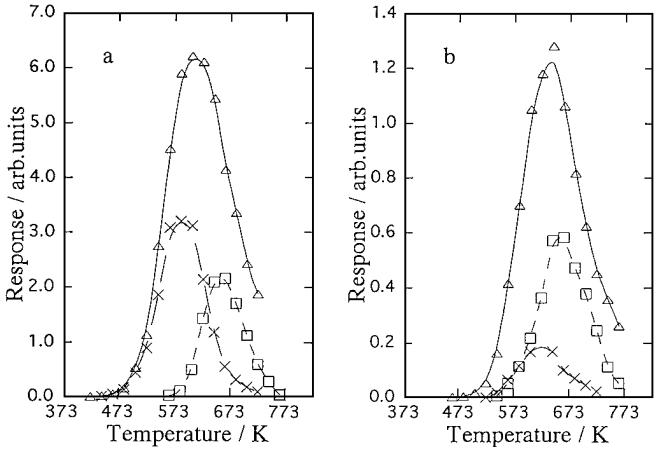


**FIG. 9.** TPD spectra after adsorption of acetic acid on catalyst B (15.0 wt%). Adsorbed amount of acetic acid: (a) saturation, (b) 0.13 times saturation. (△) carbon dioxide, (×) acetone, (□) ketene.

structure of the Zr sites in the catalyst A becomes an important factor for the catalysis.

Temperature programmed desorption was carried out on catalyst B (15.0 wt%) where acetic acid was preadsorbed at saturation and at 1/8 coverage. As shown in Fig. 9, the desorption of acetone at 580 K and of ketene at 655 K and that of carbon dioxide at 605 K were observed with the catalyst B saturated with acetic acid. The fact that ketene formation was observed at the higher temperature 75 K after acetone formation could be explained by the decomposition of acetone to ketene over empty Zr sites. When the amount of adsorbed acetic acid was much lower than saturation, the ketene formation exceeded the acetone formation as shown in Fig. 9. Ketene was not detected under the catalytic reaction conditions, where the Zr sites were saturated with bidentate acetates. In addition, the peak positions of the desorbed products shifted to higher temperatures when the amount of adsorbed acetic acid was low. This trend is characteristic of a bimolecular reaction at the surface.

If the Zr dimer site and the unsaturated coordination around the Zr atom are key issues for the catalysis, the catalyst C prepared using a Zr-dimer precursor $[(i\text{-PrCp})_2ZrH(\mu\text{-H})]_2$ was expected to be highly active. This attempt was not successful because the dimeric precursor was decomposed into a monomeric species on $SiO_2$ similar to that of the catalyst A prepared using $Cp_2ZrCl_2$ as characterized by EXAFS in Table 1. The catalytic activity of the catalyst C derived from the Zr dimer was essentially the same as that of the catalyst A as shown in Fig. 7.

## CONCLUSIONS

(1) Newly dispersed Zr catalysts A and C were prepared using $Cp_2ZrCl_2$ and $[(i\text{-PrCp})_2ZrH(\mu\text{-H})]_2$ as precursors.

(2) These catalysts were more active than catalysts B prepared from $Zr(OEt)_4$.

(3) The catalysts A and C have coordinatively unsaturated structures around the Zr atom compared to the catalyst B as characterized by XANES and EXAFS.

(4) The catalytic activity of the catalysts A increased in proportion to the square of the Zr quantity on $SiO_2$.

(5) The catalytic activity per Zr atom of catalyst B was constant up to 15.0 wt% Zr.

(6) The catalytic ketonization of acetic acid was suggested to proceed by bimolecular reaction between bidentate acetates adsorbed on Zr sites.

## REFERENCES


1. *Org. Syn. Col.* **2**, 389 (1943).
2. Kim, K. S., and Barteau, M. A., *J. Catal.* **125**, 353 (1990).
3. Kim, K. S., and Barteau, M. A., *Langmuir* **4**, 945 (1988).
4. Lee, C. C., and Spinks, J. W. T., *Can. J. Chem.* **31**, 103 (1953).
5. Sugiyama, S., Sato, K., Yamasaki, S., Kawashiro, K., and Hayashi, H., *Catal. Lett.* **14**, 127 (1992).
6. Rajadurai, S., *Catal. Rev.-Sci. Eng.* **36**, 385 (1994).
7. Koch, H., and Leibnitz, R., *Periodica Polytech* **5**, 139 (1961).
8. Neunhoeffer, O., and Paschke, P., *Chem. Ber B* **72**, 919 (1939).
9. Kwart, H., and King, K., The Chemistry of Carboxylic Acid and Esters (S. Patai, Ed.), p. 362. Interscience, New York, 1969.
10. Rubinshtein, A. M., Yakerson, V. I., and Lafer, L. I., *Kinet. Katal.* **5**, 319 (1964).
11. Vohs, J. M., and Barteau, M. A., *Surf. Sci.* **201**, 481 (1988).
12. Kuriacose, J. C., and Jungers, J. C., *Bull. Soc. Chim. Belg.* **64**, 502 (1955).
13. Imanaka, T., Tarremote, T., and Teranishi, S., *in* "5th International Congress on Catalysis, 1973," p. 163.
14. González, F., Munuera, G., and Prieto, J. A., *J. Chem. Soc. Faraday Trans. I* **74**, 1517 (1978).
15. Swaminathan, R., and Kuriacose, J. C., *J. Catal.* **16**, 357 (1970).
16. Jewur, S. S., and Kuriacose, J. C., *J. Catal.* **50**, 330 (1977).
17. Maehashi, T., Maruya, K., Domen, K., Aika, K., and Onishi, T., *Chem. Lett.*, 747 (1984).
18. Postula, W. S., Feng, Z., Philip, C. V., Akgerman, A., and Anthony, R. G., *J. Catal.* **145**, 126 (1994).
19. Nakano, Y., Iizuka, T., Hattori, H., and Tanabe, K., *J. Catal.* **57**, 1 (1979).
20. Maruya, K., Takasawa, A., Aikawa, M., Haraoka, T., Domen, K., and Onishi, K., *J. Chem. Soc. Faraday Trans.* **90**, 911 (1994).
21. Suzuki, K., and Moffat, J. B., *Catal. Lett.* **16**, 389 (1992).
22. Jackson, N. B., and Ekerdt, J. G., *J. Catal.* **126**, 31 (1990).
23. Xu, B.-Q., Yamaguchi, T., and Tanabe, K., *Chem. Lett.*, 1053 (1987).
24. Sohn, J. R., and Jang, H. J., *J. Mol. Catal.* **64**, 349 (1991).
25. Sayari, A., and Dicko, A., *J. Catal.* **145**, 561 (1994).
26. Batamack, P., Bucsi, I., Molnár, Á., and Olah, G., *Catal. Lett.* **25**, 11 (1994).
27. Jatia, A., Chang, C., MacLeod, J. D., Okubo, T., and Davis, M. E., *Catal. Lett.* **25**, 21 (1994).
28. Ziolek, M., Saur, O., Lamotte, J., and Lavalley, J.-C., *J. Chem. Soc. Faraday Trans.* **90**, 1029 (1994).
29. Babou, F., Biguot, B., and Sautet, P., *J. Phys. Chem.* **97**, 11501 (1993).
30. Chen, F. R., Coudurier, G., Joly, J.-F., and Vedrine, J. C., *J. Catal.* **143**, 616 (1993).
31. Ebitani, K., Konishi, J., and Hattori, H., *J. Catal.* **130**, 257 (1991).
32. Hino, M., and Arata, K., *Catal. Lett.* **30**, 25 (1995).

33. Yakerson, V. I., Fedorovskaya, E. A., Klyachko-Gurvich, A. L., and Rubinshtein, A. M., *Kinetika i Kataliz* **2**, 907 (1961).
34. Ichikuni, N., and Iwasawa, Y., *J. Phys. Chem*. **98**, 11576 (1994).
35. Aśakura, K., Aoki, M., and Iwasawa, Y., *Catal. Lett.* **1**, 395 (1988).
36. Iwasawa, Y., *Adv. Catal.* **35**, 87 (1987).
37. Meijers, A. C. Q., de Jong, A. M., van Gruijthuijsen, L. M. P., and Niemantsverdriet, J. W., *Appl. Catal.* **70**, 53 (1991).
38. Marquez-Alvarez, C., Fierro, J. L. G., Guerrero-Ruiz, A., and Rodriguez-Ramos, I., *J. Colloid Interface Sci.* **159**, 454 (1991).
39. Naito, S., and Tanimoto, M., *J. Catal.* **154**, 306 (1995).
40. Bosman, H. J., Kruissink, E. C., van der Spoel, J., and van den Brink, F., *J. Catal.* **148**, 660 (1994).
41. Toba, M., Mizukami, F., Niwa, S., Sano, T., Maeda, K., Annila, A., and Kommpa, V., *J. Molec. Catal.* **94**, 85 (1994).
42. Couturier, S., Tainturier, G., and Gautheron, B., *J. Organomet. Chem*. **195**, 291 (1980).
43. Rehr, J. J., Leon, J. M., Zabinsky, S. I., and Albers, R. C., *J. Am. Chem. Soc.* **113**, 5135 (1991).
44. Li, P., Chen, I.-W., and Penner-Hahn, J. E., *Phys. Rev. B* **48**, 10063 (1993).
45. Garvie, R. C., *J. Phys. Chem*. **82**, 218 (1978).
46. Smith, D. K. K., and Newkerk, H. W., *Acta. Crystallogr.* **18**, 983 (1965).
47. Teufer, G., *Acta. Crystallogr.* **15**, 1187 (1962).
48. Tanaka, T., Salama, T. M., Yamaguchi, T., and Tanabe, K., *J. Chem. Soc. Faraday Trans.* **86**, 467 (1990).
49. Asakura, K., Inukai, J., and Iwasawa, Y., *J. Phys. Chem*. **96**, 829 (1992).
50. Shirai, M., Asakura, K., and Iwasawa, Y., *J. Phys. Chem*. **95**, 9999 (1991).
51. Srinivasan, R., and Davis, B. H., *Catal. Lett.* **14**, 165 (1992).
52. Dilara, P. A., and Vohs, J. M., *Phys. Chem*. **97**, 12919 (1993).